Renal tubular Sirt1 attenuates diabetic albuminuria by epigenetically suppressing Claudin-1 overexpression in podocytes

Kazuhiro Hasegawa[1], **Shu Wakino**[1], **Petra Simic**[2], **Yusuke Sakamaki**[3], **Hitoshi Minakuchi**[1], **Keiko Fujimura**[1], **Kozi Hosoya**[1], **Motoaki Komatsu**[1], **Yuka Kaneko**[1], **Takeshi Kanda**[1], **Eiji Kubota**[3], **Hirobumi Tokuyama**[1], **Koichi Hayashi**[1], **Leonard Guarente**[2], and **Hiroshi Itoh**[1]

[1]Department of Internal Medicine, School of Medicine, Keio University, Tokyo, 160-8584, Japan

[2]Department of Biology, Massachusetts Institute of Technology, Cambridge, MA 02139, USA

[3]Department of Internal Medicine, Shizuoka Red Cross Hospital, Shizuoka, 420-0853, Japan

Abstract

The protective role of Sirt1 in renal damage was investigated. Sirt1 in proximal tubules (PT) was downregulated before albuminuria occurred in streptozotocin-induced or obese-type (*db/db*) diabetic mice. PT-specific *Sirt1* transgenic (TG) and knockout (KO) mice showed prevention and aggravation of the glomerular changes occurring in diabetes, respectively, and non-diabetic KO mice exhibited albuminuria, suggesting that Sirt1 in PT affects glomerular function. Downregulation of Sirt1 and upregulation of the tight junction protein Claudin-1 by Sirt1-mediated epigenetic regulation in podocytes contributed to albuminuria. These phenomena were not observed in 5/6 nephrectomized mice. We also demonstrated retrograde interplay from PT to glomeruli using nicotinamide mononucleotide (NMN) from conditioned medium, measurement of the auto-fluorescence of photoactivatable NMN, and injection of fluorescence-labeled NMN. In human subjects with diabetes, Sirt1 and Claudin-1 levels were correlated with proteinuria level. Sirt1 in PT protects against albuminuria in diabetes through maintaining NMN concentrations around glomeruli and controlling podocyte function.

INTRODUCTION

Diabetic nephropathy is the most common cause of end-stage renal disease, affecting about one-third of subjects with diabetes mellitus[1]. Early diabetic nephropathy is characterized by mesangial hypertrophy and glomerular hyperfiltration with microalbuminuria. Sir2 is a nicotinamide adenine dinucleotide (NAD)-dependent protein deacetylase and a member of the sirtuin class of proteins. Sirt1, a mammalian ortholog of Sir2, deacetylates histones and

various transcription factors, protecting against acute and chronic stress[2,3]. Sirt1 mitigates diabetes by attenuating hepatic insulin resistance[4,5] and enhancing pancreatic insulin secretion[6]. Recently, the renal protective effects of Sirt1[7,8] and a pathogenic role for Sirt1 in diabetic nephropathy[9–12] have been reported, although the relationship between renal Sirt1 and the pathogenesis of kidney damage in diabetes have not been investigated.

Our group recently produced transgenic (TG) mice overexpressing Sirt1 specifically in the proximal tubules (PT) and reported that Sirt1 alleviated acute kidney injury[13,14]. In diabetic nephropathy, PT changes are evident even in the early stages[15]. PT changes are reportedly closely linked to the loss of renal function and more accurately predict the progression of diabetic nephropathy than glomerular changes[15]. Therefore, our TG mice are good models for exploring the PT-specific role of Sirt1 in diabetic nephropathy. We used these mice as well as PT-specific Sirt1 knock-out mice to investigate the protective role of Sirt1 in diabetes-induced albuminuria.

RESULTS

Sirt1 in diabetes and effects of Sirt1 overexpression

Downregulation of Sirt1 expression in a diabetic milieu or high glucose condition has been reported in various cells[16,17]. We examined Sirt1 expression in PT and glomeruli after streptozotocin (STZ) treatment. By immunostaining, we detected Sirt1 expression in both PT and glomeruli before STZ treatment. Eight weeks after STZ treatment, Sirt1 levels were decreased in PTs but remained unchanged in glomeruli. Twenty-four weeks after STZ treatment, Sirt1 levels in glomeruli were also decreased (Fig. 1a). Laser micro-dissection followed by RT-PCR revealed that *Sirt1* mRNA expression decreased in PT before glomeruli in diabetic mice (Fig. 1b, Supplementary Fig. 1a,b). These observations indicated that molecular alterations in PT occurred at a very early stage in diabetes before the increase in albuminuria, as documented in several previous reports[18–20]. To delineate the significance of this change in PT, we examined the effects of Sirt1 overexpression in PT-specific *Sirt1* transgenic (TG) mice. First, we confirmed using an antibody to FLAG that TG mice overexpressed Sirt1 in PT, but not in glomeruli (Supplementary Fig. 1c). Immunoblotting, immunostaining and laser micro-dissection followed by RT-PCR all showed that the reduction in Sirt1 expression in wild-type (WT) mice at 24 weeks after STZ treatment was prevented in TG mice, in PTs and glomeruli, (Fig. 1c and Supplementary Fig. 1a,b). Plasma glucose concentrations increased in STZ-treated diabetic mice 4 weeks after treatment, in both WT and TG mice, and the increase was sustained until 24 weeks. We sacrificed mice 24 weeks after STZ treatment Supplementary Fig. 1d). Plasma glucose concentrations did not differ between WT and TG mice, at either 8 or 24 weeks (Supplementary Fig. 1d). Body weights, blood urea nitrogen and creatinine concentrations, creatinine clearance, and kidney weights did not differ between WT and TG mice Supplementary Fig. 1e–i). Eight weeks after STZ treatment, urinary albumin excretion was unchanged (Fig. 1d), although 24 weeks after treatment, urinary albumin excretion was greater in WT mice treated with STZ (WT +STZ) than in those treated with saline (Fig. 1d). This difference was less pronounced in TG mice treated with STZ (TG+STZ, Fig. 1d). Mesangial matrix accumulations were not different between WT+STZ and TG+STZ mice (Supplementary Fig. 1j). By electron

microscopy (EM), the density of tight pores was not affected by STZ at 8 weeks (Fig. 1e), although WT mice treated with STZ showed higher tight pore densities than WT mice treated with saline at 24 weeks. This difference was less pronounced in TG+STZ mice (Fig. 1e).

Sirt1-dependent upregulation of Claudin-1 expression

To elucidate the molecular mechanisms underlying the amelioration of albuminuria by PT Sirt1 overexpression, we performed DNA microarray analysis using micro-dissected glomerular regions to examine differences in gene expression between WT+STZ and TG +STZ mice. In the Welch *t*-test with a cutoff of *P* < 0.05, 26 genes showed a statistically significant upregulation greater than 4-fold in TG mice (Supplementary Table 1) and 29 genes showed downregulation in TG mice to 25% of the level in WT mice (Supplementary Table 2). We selected four upregulated genes and four downregulated genes for which the functions were known and confirmed the differential expression of these genes by quantitative real-time RT-PCR using whole kidney samples (Supplementary Fig. 2). Only *Claudin-1* showed a significant reduction in mRNA level in STZ+TG mice compared with STZ+WT mice. In addition, among the eight genes, *Claudin-1* was reported to be the most related to the pathogenesis of albuminuria[21,22]. Therefore, we focused on the changes in Claudin-1 expression.

Expression of *Claudin-1* mRNA, a putative parietal epithelial cell (PEC)-specific marker[23–25], was higher in WT+STZ mice than in saline-treated WT mice (WT+Sal). This difference was not seen in TG mice (Fig. 1f). By microarray analysis, no other isoforms of Claudin were upregulated or downregulated. By immunostaining, Claudin-1 appeared to be expressed only in PECs in WT+Sal mice (Fig. 1g). Claudin-1 levels were higher in WT +STZ mice than in WT+Sal mice, and Claudin-1 extended ectopically in podocytes (Fig. 1g). This difference in Claudin-1 levels in both PECs and podocytes was not seen in TG mice (Fig. 1g). Laser micro-dissection followed by real-time PCR revealed lower levels of *Sirt1* mRNA expression in PECs and PT cells of WT+STZ mice than in those of WT+Sal mice (Fig. 1h). *Claudin-1* mRNA expression was substantially higher in PECs of WT+STZ mice compared with those of WT+Sal mice, although we detected little *Claudin-1* expression in PT cells of WT+Sal and WT+STZ mice (Fig. 1h). In TG mice, *Sirt1* mRNA expression levels were unaffected by STZ in either PT or PECs (Fig. 1i). We detected little expression of *Claudin-1* in PT and PECs, and its expression in these regions was unaffected by STZ (Fig. 1i). Finally, in immunogold EM of the foot processes of podocytes, we did not observe gold particles for Claudin-1 in WT+Sal mice, while we observed large numbers in WT+STZ mice. This difference was not seen in TG mice (Supplementary Fig. 3a–c). Collectively, these findings suggested that Sirt1 overexpression in PT altered Claudin-1 expression in PECs as well as in podocytes, but not in PT cells.

Effects of Claudin-1 expression in podocytes

To examine the effects of Claudin-1 on albuminuria, we transferred a construct containing the *Claudin-1* gene inserted downstream of a podocyte-specific promoter, a 2.5-kb fragment of the *NPHS2* (*podocin*) promoter, into WT mice with the aid of a hemagglutinating virus of Japan envelope vector[26]. Injection of the *Claudin-1* gene driven by a *Podocin* promoter

successfully upregulated Claudin-1 expression in podocytes (Fig. 2a). This gene transfer induced albuminuria in WT mice and aggravated albuminuria in STZ-treated mice (Fig. 2b). These effects were accompanied by greater podocyte effacement (Fig. 2c).

The β-catenin/Snail pathway plays a role in the pathogenesis of albuminuria[27], and Claudin-1 reportedly activates the β-catenin/Snail pathway in colon epithelial cells[28]. Thus, we examined whether Claudin-1 activated the β-catenin/Snail pathway in podocytes. Transfer of *Claudin-1* gene upregulated both β-*catenin* and *Snail* mRNA levels concomitantly with downregulation of the mRNAs for the slit membrane protein Podocin and the actin-binding protein Synaptopodin in micro-dissected glomeruli (Fig. 2d). Overexpression of Claudin-1 was also associated with increased expression of β-catenin and Snail, and downregulated synaptopodin expression in cultured podocytes (Fig. 2e). Collectively, these findings suggest that Claudin-1 expression in podocytes induced podocyte effacement and led to albuminuria, presumably through the activation of β-catenin/ Snail signaling.

Deficiency of Sirt1 in proximal tubules causes albuminuria

To confirm the role of PT Sirt1 in albuminuria in diabetes, we also created PT-specific *Sirt1*-deficient mice (conditional knockout mice, CKO) by crossing *Sirt1*^flox/flox mice on a C57BL/6J background with γ*GT*-Cre mice. CKO mice showed specific loss of Sirt1 expression in the kidney (Fig. 2f). Immunofluorescence staining revealed that control littermates aged 8 weeks expressed Sirt1 in the glomeruli and tubules in kidney tissues. In CKO mice, we observed almost complete elimination of Sirt1 expression in tubules, whereas glomerular expression was unaffected, denoting a tubular-specific knockout of *Sirt1* (Supplementary Fig. 4a).

We then compared phenotypes in 32-week-old mice (24 weeks after saline or STZ treatment). Micro-dissection followed by real-time PCR revealed lower PT *Sirt1* expression levels in CKO mice than in control mice (Fig. 2g, Cont+Saline vs. CKO+Saline). Of note, levels in glomeruli were also lower (Fig. 2g, Cont+Saline vs. CKO+Saline). *Sirt1* expression levels in PTs and glomeruli were also lower in control mice treated with STZ (Cont+STZ) and CKO mice treated with saline (CKO+Saline) than in control mice treated with saline (Cont+Saline). This difference was more prominent in CKO mice treated with STZ (CKO +STZ) (Fig. 2g). The results of immunofluorescence staining (Supplementary Fig. 4a) were consistent with those of real-time PCR. By EM, the density of tight pores was higher in Cont +STZ and CKO+Saline mice than in Cont+Saline mice. An even higher tight pore density was seen in CKO+STZ mice (Fig. 2h). Immunostaining (Fig. 2i), real-time PCR after laser micro-dissection (Fig. 2i), and immunogold electron microscopy (Supplementary Fig. 4b) revealed higher levels of Claudin-1 expression in Cont+STZ and CKO+Saline mice compared with Cont+Saline mice, an effect that was further enhanced in CKO+STZ mice. Urinary albumin excretion was greater in Cont+STZ and CKO+Saline mice than in Cont +Saline mice, and higher again in CKO+ STZ mice (Fig. 2j). These data from PT-specific *Sirt1*-deficient mice confirmed the pivotal role of endogenous PT Sirt1 in maintaining glomerular structure and function during the initiation of albuminuria in diabetes as well as in the normal condition.

Sirt1 overexpression in obese and nephrectomized mice

We further investigated the effects of Sirt1 overexpression in PT in another diabetic model and 5/6 nephrectomized (5/6Nx) mice. We crossed our *Sirt1* TG mice with obese *db/db* mice and produced Sirt1 TG-*db/db* mice (TG-*db/db*). Plasma glucose concentrations and body weights were significantly greater in WT-*db/db* mice (WT-*db/db*) and TG-*db/db* mice than in nondiabetic (ND) mice. Plasma glucose concentrations were already elevated at 8 weeks of age, and this elevation was sustained until 32 weeks of age (Supplementary Fig. 4c). Body weights, blood urea nitrogen and creatinine concentrations, creatinine clearance, and kidney/body weight ratios did not differ between WT-*db/db* and TG-*db/db* groups (Supplementary Fig. 4d–h). Sirt1 expression in WT-*db/db* mice was lower than that in WT-ND mice, but there was no significant difference in Sirt1 expression levels between TG-ND mice and TG-*db/db* mice (Fig. 3a). Urinary albumin excretion, Claudin-1 levels, and the density of tight pores did not differ between 32-week-old TG-ND mice and WT-ND mice. However, these parameters were greater in WT-*db/db* mice than in either type of ND mice at 32 weeks of age when glomerular lesions were evident. In TG-*db/db* mice, no such difference was observed (Fig. 3b–d). PAS staining revealed an increase in mesangial matrix accumulation in diabetic groups, but there was no difference between WT-*db/db* and TG-*db/db* mice (Supplementary Fig. 4i).

To explore the role of renal tubular Sirt1 in non-diabetes-related albuminuria, we performed similar experiments using 5/6Nx mice[29]. Twenty-four weeks after nephrectomy, the expression of Sirt1 was unchanged, and PT-specific *Sirt1* TG mice expressed high levels of Sirt1 in the kidney (Fig. 3e). The 5/6Nx mice exhibited albuminuria to a level that was similar to that in STZ-treated mice. However, PT-specific Sirt1 overexpression could not prevent albuminuria in 5/6Nx mice (Fig. 3f). Collectively, these data indicated that the effect of PT Sirt1 in preventing albuminuria is a diabetes-specific event.

Epigenetic mechanism of Sirt1-induced Claudin-1 upregulation

We further explored the mechanism regulating Claudin-1 expression using human-derived renal epithelial (HRE) cells because this cell line expresses Claudin-1 and has a similar phenotype to that of PECs. Sirt1 expression decreased and Claudin-1 expression increased as the glucose concentration increased (Fig. 4a). Transfection of cells with an increased amount of Sirt1 expression vectors resulted in downregulation of Claudin-1 expression (Fig. 4b). Sirt1 overexpression blunted the upregulation of Claudin-1 by glucose (Fig. 4b). We investigated the epigenetic mechanisms for regulating Claudin-1 expression[30]. A computer search indicated that CpG islands, a target for methylation, reside within the *Claudin-1* genes of both mice and humans (Fig. 4c). Methylation analysis revealed that the amount of methylated CpG decreased with increasing glucose concentration in concert with the upregulation of Claudin-1 (Fig. 4d). The transfection of cells with increased concentrations of Sirt1 expression vectors induced hypermethylation of the *Claudin-1* gene in concert with the downregulation of Claudin-1 (Fig. 4 d). Transfection of cells with an siRNA for *Sirt1* induced hypomethylation of the *Claudin-1* gene and upregulated Claudin-1 expression (Fig. 4e). Sirt1 overexpression blunted the hypomethylation of *Claudin-1* gene CpG islands induced by glucose (Fig. 4f).

Treatment of cells with 5-aza-dC, a DNA methyltransferase (Dnmt) inhibitor, reduced the level of methylation of the *Claudin-1* gene and increased Claudin-1 protein levels (Fig. 4g). The methylation of the *Claudin-1* CpG region induced by overexpression of Sirt1 was suppressed by co-transfection of cells with an siRNA for *Dnmt1* (Fig. 4h), but not by co-transfection of cells with siRNAs for *Dnmt3a* and *Dnmt3b* (Supplementary Fig. 5a,b). In an inactivation model of gene expression, histone deacetylation induces histone methylation, which leads to the recruitment of Dnmt[31,32]. We examined chromatin modification status by chromatin immunoprecipitation (ChIP) assays to confirm the molecular events in the CpG islands in the *Claudin-1* gene[33,34]. Acetylation of both H3 and H4 histones was greater in both CpG and non-CpG regions in cells treated with sirtinol, a Sirt1 inhibitor, than in control cells (Fig. 4i). Histone H3K9 dimethylation in the CpG region was decreased by sirtinol, although histone H4K20 dimethylation was unaffected by sirtinol treatment (Fig. 4i). These results suggested that Sirt1 deacetylated H3 and H4 histones in both CpG and non-CpG regions and enhanced dimethylation of H3K9 in CpG regions (Fig. 4i). They also indicated that Claudin-1 expression was regulated epigenetically through deacetylation of histone H3 and H4 by Sirt1, with subsequent CpG methylation of the *Claudin-1* gene by recruited *Dnmt1*.

We confirmed these epigenetic changes in PECs micro-dissected from STZ-treated *Sirt1* TG mice. Diabetes-induced hypomethylation of *Claudin-1* CpG regions and Sirt1 overexpression led to higher levels of methylation of these regions (Fig. 4j). In parallel with these epigenetic changes, the levels of *Claudin-1* mRNA expression were higher in WT +STZ mice than in TG+STZ mice (Fig. 4j). We obtained more quantitative results by bisulfite sequencing using micro-dissected PECs (Supplementary Fig. 5c,d).

Interaction between PT cells and podocytes through nicotinamide mononucleotide

Our data indicated that the phenotype changes in PT cells affected contiguous cells including podocytes. We examined this interaction between PT cells and podocytes in conditioned medium (CM) experiments. We transfected a human renal PT cell line, HK-2 cells, cultured either in normal (NG) or high glucose (HG) conditions, with Sirt1 expression vectors (Fig. 5a). We obtained CM from these cells and treated podocytes with or without these conditioned media. Podocytes cultured without CM expressed Sirt1 protein but had undetectable levels of Claudin-1 protein. In the absence of CM, HG culture conditions did not change the levels of these molecules. However, CM from HK-2 cells cultured in NG conditions induced higher levels of Sirt1 expression in podocytes. Exposure of podocytes to CM from HK-2 cells cultured in HG conditions (HG+Cont) downregulated Sirt1 and upregulated Claudin-1 in podocytes. These effects were diminished in podocytes exposed to CM from HK-2 cells transfected with Sirt1 expression vector and cultured in HG conditions (Fig. 5b). Thus, CM from HK2 cells contained some factor responsible for the Sirt1 expression alteration in podocytes.

Nicotinic acid metabolites are candidates for this effect because they are related to Sirt1 expression[35] and activity[36,37]. In this metabolic pathway, nicotinamide (NAM) is converted into nicotinamide mononucleotide (NMN) by intracellular-type NAM phosphoribosyltransferase (iNAMPT). NMN is further converted into NAD by nicotinamide

mononucleotide adenylyl transferase (NMNAT). NAD is then converted by Sirt1 into NAM, forming a metabolic loop[36,38]. In our culture system, NMN concentrations and the NAD/NADH ratio were lower in CM from HK-2 cells cultured in the HG condition than in CM from HK-2 cells cultured in the NG condition. We did not observe such a difference in CM from Sirt1-transfected HK-2 cells (Fig. 5c). Exogenous supplementation of NMN into CM from HK-2 cells cultured in the HG condition induced higher levels of Sirt1 and lower levels of Claudin-1 in podocytes. Sirtinol abrogated these effects of NMN treatment (Fig. 5d). We did not observe these molecular changes when we used mannitol in the place of glucose, indicating that osmotic changes had no effects (Supplementary Fig. 6a–f. For details, see Supplementary Results). Collectively, these findings suggested that Sirt1 prevented the HG-induced decrease in NMN and NAD concentrations in CM, which could, at least in part, have contributed to the changes in Sirt1 expression and probably the subsequent alteration of Claudin-1 expression in podocytes. We measured NMN concentrations inside the cells in CM experiments. NMN photoactivated by pretreatment with perchloric acid and acetophenone at high temperature[39] was detected in HK-2 cells (Fig. 5e). HK-2 cells cultured in HG contained lower concentrations of NMN than did those cultured in NG (Fig. 5e). This difference was reversed in HK-2 cells transfected with the Sirt1 expression vector. In podocytes, basal concentrations of NMN were almost undetectable (Fig. 5e). One and 2 h after exposure to normal glucose CM, NMN concentrations inside podocytes were higher. The NMN concentration was low when we treated podocytes with high glucose CM, but was higher in podocytes treated with CM from Sirt1-transfected HK-2 cells (Fig. 5e). These data indicated that NMN synthesized and secreted by HK-2 cells was taken up by podocytes. Next, we directly measured tissue NMN concentrations in kidneys using this method. We detected NMN mainly in tubular regions (Fig. 5f), probably because of the high expression levels of the NMN-producing enzyme iNampt (Fig. 5g). NMN levels were lower in WT mice treated with STZ than in WT mice treated with saline (Sal), and this difference was less apparent in *Sirt1* TG mice (Fig. 5f). Consistently, weaker immunostaining for iNampt was seen in WT+STZ mice compared with WT+Saline mice, while stronger immunostaining was seen in TG+STZ mice compared with TG+Saline mice (Fig. 5g). Similarly, in CKO mice, NMN concentrations were lower in Cont+STZ and CKO+Sal mice than in Cont+Sal mice, and lower still in CKO+STZ mice (Supplementary Fig. 6g). Immunostaining for iNampt was weaker in Cont+STZ and CKO+Sal mice than in Cont+Sal mice, and weaker still in CKO+STZ mice (Supplementary Fig. 6h). These results suggested that iNampt levels were affected, at least in part, by glucose or by the Sirt1-determined tissue NMN concentrations around PT, which regulated Sirt1 and Claudin-1 expression levels in podocytes.

To confirm a role for NMN in the progression of diabetes-induced albuminuria, we examined the effects of FK866, an inhibitor of iNampt. FK866 at the dose of 30 mg kg^{-1} decreased NMN concentrations (Supplementary Fig. 7a), leading to higher levels of Claudin-1 expression (Supplementary Fig. 7b) and albuminuria (Supplementary Fig. 7c). EM revealed that FK866 induced higher tight slit pore density and Claudin-1 levels in podocytes (Supplementary Fig. 7d,e).

Our data implied a pivotal role for the molecular interplay between iNampt/NMN in PT and Sirt1/Claudin-1 in podocytes in diabetes-induced albuminuria. We investigated retrograde interplay from tubular cells to podocytes in an *in vivo* system. N-methylanthraniloyl (Mant)-NMN is an autoimaging substance that cannot be synthesized endogenously[40,41]. One hour after injection into the renal artery Mant-NMN accumulated in tubules, and 2 h after injection its accumulation could be detected in glomeruli (Fig. 5h). These temporal changes in the localization of Mant-NMN strongly suggested that NMN was taken up by tubular cells and thereafter delivered into glomeruli. In CKO mice that lack the ability to supply NMN to glomeruli from proximal tubules, the late peak in podocytes was almost abolished (Fig. 5i). This result supported the hypothesis that the NMN accumulation in podocytes was derived from proximal tubules and not from slow accumulation in glomeruli. However, we need to further investigate the detailed mechanisms underlying NMN secretion or absorption. Presumably, NMN absorption in podocytes will depend on nucleotide receptors such as P2X or P2Y[42].

Sirt1 and Claudin-1 expression in human renal biopsy samples

We evaluated renal the expression of Sirt1 and Claudin-1 in human specimens from 11 subjects with diabetes (Supplementary Table 3). Sirt1 expression in both PT and glomerular regions was lower, and Claudin-1 expression in the glomerular region was higher, in the kidneys of subjects with heavy proteinuria (12 g d^{-1}) compared with those with moderate proteinuria (1.5 g d^{-1}) (Fig. 6a). Claudin-1 expression was negatively correlated with Sirt1 expression in both PT and glomerular regions (Fig. 6b).

Among several clinical parameters, only proteinuria was correlated with both PT and glomerular Sirt1 immunostaining, and also with glomerular Claudin-1 immunostaining (Fig. 6c). There were no correlations between eGFR and immunostaining patterns for either protein (Fig. 6d).

DISCUSSION

Our data revealed that reduced Sirt1 expression in PT led to reduced Sirt1 levels and higher Claudin-1 levels in glomeruli, leading to the initiation of albuminuria in diabetic model mice. These findings indicated a protective role for PT Sirt1 against albuminuria that is specific for diabetes-induced albuminuria.

We also showed direct epigenetic regulation of *Claudin-1* gene expression by Sirt1. The significant role of Dnmt1 in Sirt1-induced gene methylation in the present study is consistent with a recent study showing that Sirt1 directly deacetylated and activated Dnmt1[43]. The results in our PT-specific gene engineered mice implied that the molecular changes in PT induced the phenotype changes in glomeruli and podocytes.

We also showed a role for NMN as a candidate mediator of the interplay between PT cells and podocytes. This retrograde interplay was confirmed by tracing photoactivated labeled NMN both *in vitro* and *in vivo*. Our data suggest that NMN derived from PT cells is absorbed by podocytes; however, more work is needed to confirm this hypothesis (Supplementary Fig. 8).

Finally, we showed that expression of Sirt1 and Claudin-1 was correlated with levels of proteinuria in human renal biopsy samples from subjects with diabetes. Because neither of our diabetic mouse models developed significant diabetic nephropathy, we should interpret the present data carefully. In addition, the mechanisms regulating NMN concentrations in PT based on glucose condition or Sirt1 expression level remain unclear. However, because the clinical data are consistent with the results obtained from mouse models, we suggest that initial downregulation of Sirt1 expression in PT, followed by downregulation of Sirt1 and upregulation of Claudin-1 in glomeruli, has a role in the initial changes in diabetes-induced albuminuria[44]. The results of this study could contribute to novel therapeutic strategies to prevent diabetes-induced albuminuria.

METHODS

Production of *Sirt1*-TG mice (TG mice) and kidney-specific *Sirt1* knockout mice (CKO mice)

To prepare renal tubule-specific *Sirt1* TG mice on a C57BL/6J background, a transgenic expression vector containing a mouse sodium phosphate cotransporter IIa (*Npt2*) promoter and human *Sirt1* cDNA tagged with an 8-amino acid FLAG epitope was constructed as described previously[14]. Immunostaining using an antibody to FLAG showed expression of the transgene in PT but not in glomeruli (Supplementary Fig. 1c). Mice were propagated as heterozygous transgenic mice by breeding them with WT C57BL/6 mice. F2 mice were used as TG mice, and age- and sex-matched littermates were used as wild-type control (WT) mice. Kidney-specific *Sirt1* knockout (*Sirt1*$^{-/-}$) mice (CKO mice) were produced by crossing *Sirt1*$^{flox/flox}$ mice on a C57BL/6J background with γ*GT*-Cre mice (Jackson Laboratory)[45]. γ*GT*-Cre transgenic mice on a C57BL/6J background have demonstrated PT-specific Cre recombinase activity[2]. Therefore, *Sirt1*$^{flox/flox}$/γ*GT*-Cre$^{tg/+}$ (PT-specific *Sirt1*$^{-/-}$) mice had a specific deletion of *Sirt1* in PTs. The following three types of control mice were produced by this breeding: *Sirt1*$^{flox/flox}$, *Sirt1*$^{+/+}$/γ*GT*-Cre$^{tg/+}$, and *Sirt1*$^{+/+}$. In the following studies, *Sirt1*$^{flox/flox}$/γ*GT*-Cre$^{tg/+}$ were crossed with *Sirt1*$^{flox/flox}$ to produce *Sirt1*$^{flox/flox}$/γ*GT*-Cre$^{tg/+}$ (PT-specific *Sirt1*$^{-/-}$) mice. *Sirt1*$^{flox/flox}$ mice were used as control (Cont) mice. All animal studies were performed in accordance with the animal experimentation guidelines of Keio University School of Medicine.

Podocyte-specific Claudin-1 overexpression in mice

Mouse *Claudin-1* cDNA was cloned as described previously[46]. The cDNA was inserted downstream of a podoyte-specific promoter, a 2.5-kb fragment of the human *NPHS2* (*Podocin*) promoter[47]. Eight-week-old male mice were treated with saline or STZ. One week after saline or STZ injection, 50 μg of 2.5 AU hemagglutination virus of Japan (HVJ)-envelope vector (GenomeONE-Neo, Ishihara Sangyo, Osaka, Japan) that carried plasmid DNA was injected into the tail vein in 120 μl of suspension buffer weekly. Mice were killed 24 weeks after injection.

Experimental protocol for animal experiments

STZ treatment—Eight-week-old male mice were treated with streptozotocin (STZ, Sigma-Aldrich, St. Louis, MO) dissolved in 100 mmol l^{-1} citrate buffer, pH 4.5, or with phosphate-buffered saline (PBS) dissolved in citrate buffer.

***db/db* mice**—To produce compound mutant mice with a Sirt TG *db/db* genotype, PT-specific *Sirt1* TG (TG) mice were bred with male mice heterozygous for the *db* mutation (*db/m*). Both the *Sirt1* TG and *db* heterozygous breeders were on a C57BL/6J genetic background. Offspring from the F1 generation, which were heterozygous for the *db* mutation and also expressed the *Sirt1* transgene, were then bred with mice heterozygous for the *db* mutation. The F2 generation contained the desired compound mutant (*Sirt*-Tg, *db/db*) and the other genotypes used. The following four genotypes were used: *1*) wild-type nontransgenic (WT)-nondiabetic (ND); *2*) WT-*db/db; 3*) TG-ND; and *4*) TG-*db/db*. At the age of 6 months, mice were sacrificed.

5/6 Nephrectomy—Eight-week-old male C57BL/6 mice were subjected to 5/6 nephrectomy in two stages[29]. In the first stage, the left kidney was decapsulated, and then the upper and lower poles were partially resected via a left flank incision. After one week, the entire right kidney was removed[5]. Sham operated mice were used as controls. Twenty-four weeks after the surgery, kidney tissues were harvested.

FK866 treatment—FK866 (Sigma, St Louis, MO) was dissolved in dimethyl sulfoxide and 25 mg ml^{-1} aliquots were stored at -80 °C until further use. Male C57BL/6 mice received intraperitoneal injections of 30 mg kg^{-1} FK866 further diluted in PBS twice a day 3 d a week from 8 weeks to 32 weeks of age.

Histopathological examination—PAS-stained samples from 30 consecutive glomeruli per animal were examined. The glomerular area was traced along the outline of the capillary loop using Image-Pro Plus 3.0 (Media Cybernetics, Silver Spring, MD). The extent of the mesangial matrix was determined by assessment of the PAS-positive and nucleus-free areas in the mesangium. Immunohistochemistry was performed as previously described[14]. Briefly, paraffin sections (4 μm) were fixed in 3% formaldehyde and stained using primary antibodies against FLAG (Sigma), Sirt1 (Millipore, Bedford, MA), Claudin-1 (Invitrogen, San Diego, CA). The sections were stained with biotin-labeled goat anti-rabbit IgG (Vector) or biotin-labeled anti-mouse IgG (Vector) and then treated with the Vectastain Elite ABC Kit (Vector).

Immunofluorescence staining—Indirect immunofluorescence staining for Sirt1 was carried out on frozen kidney sections using rabbit monoclonal anti-Sirt1 antibody (Cell Signaling Technology). Alexa Fluor goat anti-rabbit IgG (Molecular Probes, Eugene, OR, USA) was used as the secondary antibody. As a negative control, the primary antibody was replaced with nonimmune serum from the same species; no staining occurred. Immunofluorescence staining for AQP1 was performed in a similar manner using respective antibodies. For fluorescence microscopy, all sections were stained and analyzed at the same time to exclude artifacts due to variable decay of the fluorochrome. Sections were examined

using a Nikon Microphot-FX fluorescence microscope equipped with a Spot II digital camera.

Electron microscopy—For electron microscopy evaluation, kidney tissue was embedded in Epon epoxy resin (Miller-Stephenson Chemical Company, Sylmar, CA)[48]. Electron micrographs of 10 glomeruli per kidney were randomly taken for each mouse to evaluate podocyte morphometry. Photomicrographs of the GBM were analyzed for the density of tight slit pores between the podocyte foot processes according to published methods[6]. Tight slit pores were identified by the obliteration of spaces between adjacent foot processes. The numbers of tight slit pores were counted and divided by the GBM length (mm) to determine the density of tight slit pores. A total of 500 foot processes from each group were evaluated for the analysis of slit pore density.

Immunogold electron microscopy—Mouse kidneys from the four groups were finely chopped, fixed in 4% paraformaldehyde and 0.2% picric acid, and embedded in LR white resin. Ultrathin sections were blocked with goat IgG and incubated with rabbit anti-Claudin-1 (Invitrogen) followed by 15 nm colloidal gold-conjugated goat anti-rabbit IgG (EBS, East Granby, CT). Grids were counterstained with 0.5% osmium and 1% uranyl acetate, and bound gold particles were visualized and photographed by electron microscopy. The numbers of gold particles μm^{-2} were then counted using Scion software, and averages were compared statistically.

Laser microdissection—Laser microdissection was performed according to previous reports[49,50]. We used poly-L-lysine to prevent PECs (kindly provided by Professor Stuart J. Shankland and Cheri Campbell, Division of Nephrology, University of Washington) from detaching from glass slides and a modified PAS staining protocol specific for laser microdissection samples from cryosections, not generally used on paraffin-embedded samples. Freshly frozen kidney tissue was cut into 7-μm-thick sections. Cryosections were mounted onto a polyethylene membrane previously attached to a glass slide that had been coated with 0.1% poly-L-lysine (Sigma-Aldrich). The sections were stained with PAS, counterstained with hematoxylin, and stored at −80 °C until use. These tissues were excised using a PALM MicroBeam IP 230V Z microscope for laser pressure catapulting (P.A.L.M. Microlaser Technologies, Bernried Germany) as described previously[50]. RNA from microdissected tissue was prepared using the PALM RNA extraction kit.

Microarray Analysis—Mice in the WT+STZ and TG+STZ groups were killed at 32 weeks of age. Before microarray analysis, we dissected the glomerular regions. Micro-dissected glomeruli were immediately used for total RNA isolation and subjected to analysis on Affymetrix Mouse Genome 430 2.0 microarray chips according to Affymetrix standard protocols (http://www.affymetrix.com). Genes were excluded if the signal strength did not significantly exceed background values and if expression did not reach a threshold value for reliable detection ($P < 0.05$) in each of the 3 separate studies. Finally, genes were excluded if the level of expression did not vary by more than 4-fold or less than 0.25-fold between WT+STZ and Tg+STZ. The remaining genes were subjected to nonparametric Welch *t*-tests and are reported with their respective fold changes and *P*-values.

Culture of podocytes and HK-2 cells—Conditionally immortalized mouse podocytes were donated by P. Mundel (Mt. Sinai School of Medicine, New York, NY, USA) and K. Asanuma (Juntendo University, Tokyo, Japan)[51]. Mouse *Claudin-1* cDNA was cloned as described previously[46]. In conditioned medium experiments, control or Sirt1 vector transfected HK2 cells seeded at a density of 5×10^5 100 mm^{-2} were cultured for 24 h with either normal glucose (5 mM, NG) or high glucose (25 mM, HG). The conditioned medium from each treatment was then transferred onto culture plates containing podocytes. DMEM containing 10% FBS was used for both cell types. Podocytes were seeded at a density of 5×10^5 100 mm^{-2}, incubated for 7 d (differentiation) and used for experiments. Differentiation of cells was confirmed as previously described[51]. The NAD$^+$/NADH ratio was measured in whole cell extracts of HK2 cells or podocytes using the BioVision NAD/NADH Quantitation Kit (BioVision, Mountain View, CA). NMN was detected by high-performance liquid chromatography (HPLC) as previously described[39].

Culture of HRE cells—Primary HRE cells (Clonetics, San Diego, CA) were cultured according to the manufacturer's instruction. The expression plasmid containing human *Sirt1* cDNA (pcDNA3.1-Sirt1) and the control plasmid (pcDNA3.1) were transfected into HRE cells using Lipofectamine 2000 (Invitrogen). For treatment with 5-Aza-dC (Sigma-Aldrich), the cells were treated with 5 μM 5-aza-dC for 96 h. For *Dnmt* siRNA treatment, *Dnmt* siRNA duplex was purchased from Sigma-Aldrich. The sense sequences were 5′-[dT] GGAAUGGCAGAUGCCAACAGC [dT]-3′ for Dnmt1, 5′-[dT] GAAAGCGAAGGUCAUUGCA [dT]-3′ for Dnmt3a, and 5′-[dT] GCUAGCGAAGGUCAUUGCA [dT]-3′ for Dnmt3b. Control siRNA consisted of a scrambled siRNA construct encoding a nonspecific siRNA without mammalian homology. These siRNAs (100 pmol μl^{-1}) were transfected using Lipofectamine 2000 (Invitrogen) for 24 h.

RNA isolation, reverse transcription, and quantitative PCR—Real-time PCR was performed using the ABI Prism 7700 sequence detection system (Applied Biosystems, Foster City, CA) and the SYBR GREEN system (Applied Biosystems)[13,14]. The sequences of the primers are listed in Supplementary Table 5. The relative mRNA levels for the specific genes were normalized to the level of mRNA expression for the housekeeping gene *GAPDH*.

Immunoblotting—Immunoblotting was performed as described previously[13,14] using specific antibodies against Sirt1 (Millipore) and Claudin-1 (Invitrogen). For assaying β-catenin/Snail signaling, an anti-Synaptopodin primary antibody (Sigma, St Louis, MO; Biodesign, Sabo, ME), anti-β-catenin antibody (catalog number 610154; BD Transduction Laboratories, San Jose, California), and anti-Snail antibody (ab17732; Abcam) were used. The β-actin band recognized by a specific antibody (Sigma) was used as a loading control. Band intensities were quantified using Scion Image Software (Scion Corp, Frederick, MD).

Claudin-1 CpG methylation in vivo by methylation-specific PCR (MSP) and real-time methylation-specific PCR (real-time MSP)—Total genomic DNA from the kidneys or HRE cells was extracted using a DNeasy Kit (Qiagen Japan, Tokyo). Bisulfite

conversion of genomic DNA was performed using a Zymo EZ DNA Methylation Gold™ kit (Zymo Research Corp., Orange, CA). MSP was performed to determine the methylation status of the *Claudin-1* gene, and real-time MSP was performed for quantitative analysis of the methylation of the *Claudin-1* gene as described previously[11]. Specific methylated or unmethylated sequences of primer sets are listed in Supplementary Table 6. Two independent bisulfite modifications were performed, and five independent MSPs and real-time MSPs were performed. Representative bands of MSP are shown in the figures[52].

Bisulfite genomic sequencing—DNA was extracted from cells according to standard procedures. A 2-μg quantity of DNA was then bisulfite treated using the EpiTect Bisulfite Kit (Qiagen) and amplified via nested PCR using the following PCR primers. PCR1 forward: 5′-AGTTGTATAGAGAGTAAGGGTATAGGT-3′, reverse: 5′-TTAACCTAAAACTTAAATTCTTTCTAC-3′, PCR2 forward: 5′-AGGTATTAATT TGTTTGTAGAGATT-3′, reverse: 5′-TAACCTCTAAACTAAATAAAACTACTACA-3′. PCR products were cloned using the TOPO TA cloning kit (Invitrogen). Ten random clones were sequenced using an ABI3730 DNA analyzer (Applied Biosystems) with the following sequence primers; forward: 5′-CAGGAAACAGCTATGAC-3′, reverse: 5′-GTTTTCCCAGTCACGACGT-3′.

Sirt1 small interfering RNA (siRNA) experiments—The siRNA for *Sirt1* was prepared by Japan Bio Service (JBios, Saitama, Japan). The targeted sequence to silence the transcription of Sirt1 was 5′-GAAGTTGACCTCCTCATTG-3′. An siRNA targeting sequence for green fluorescent protein (GFP; 5′-GGCTACGTCCAGCAGCGCACC-3′) mRNA was used as a negative control. As another negative control, a scrambled siRNA (JBioS) that did not exhibit homology to any coding region was used. The sequence: 5′-TCCGAACGTGGCACGA-3′ was used as the scrambled siRNA control.

Chromatin Immunoprecipitation (ChIP) assay—HRE cells were treated with or without the Sirt1 inhibitor sirtinol (20 μM, 48 h, Sigma-Aldrich) for 48 h and used for the following ChIP assay. The ChIP assay was performed with 1×10^6 HRE cells per assay using the ChIP assay kit (Upstate Biotechnology Inc., Lake Placid, NY) as described by the manufacturer's protocol. All antibodies used in this study were purchased from Abcam. Antibodies against acetylated histone H3, acetylated histone H4, dimethylated H3K9, dimethylated H3K27, and dimethylated H4K20 were used for immunoprecipitation (IP), and rabbit IgG was used as a negative control to check the specificity of IP. After IP, recovered chromatin samples were subjected to PCR with the following set of primers: AACTCTCCGCCTTCTGCAC and ACACGCAGGACATCCACAG for the CpG region of *Claudin-1* and CCGTTGGCATGAAGTGT ATG and AAGGCAGAGAGAAGCAGCAG for the non-CpG region of *Claudin-1*. The PCR products were run on agarose gels. The results from three independent experiments are presented.

Quantification of NMN autofluorescence by photoactivatable NMN—Intracellular endogenous NMN autofluorescence was monitored by confocal microscopy as described previously[39] with slight modification. Briefly, 100 ml of 1 N $HClO_4$ was added to cells or kidney sections on a culture dish or a glass plate. Then, these sections were embedded with

1 N KOH and, after 5 min, an additional 100 ml of 0.1 M bicine pH 7.4 was added, followed by 1 N KOH and acetophenone. These samples were incubated for 15 min, and then 100 ml formic acid was added. By means of this derivatization procedure, NMN shows fluorescence with peaks of excitation and emission in the regions of 332 nm and 454 nm, respectively. A confocal microscope equipped with a custom 340 ± 10 nm excitation and 460 ± 25 nm emission filter set was used together with a Zeiss Axiocam digital camera (Carl Zeiss) for imaging intrinsic NMN autofluorescence from HK2 cells, podocytes, or kidney sections freshly isolated from each mouse. Collected images were subsequently analyzed using Zeiss Axiovision 4.4 software. Background fluorescence intensity was subtracted from each data point.

Synthesis of Mant-NMN and intra-renal artery injection of Mant NMN—To elucidate whether NMN is released from PTs and then mobilized into podocytes, fluorescence-labeled exogenous NMN was injected into mice. We used Mant (N-methylanthraniloyl) for labeling NMN. Mant-NMN was synthesized as described[39,40]. Saline or Mant-NMN (500 mg kg^{-1} body weight) was administered by intra-arterial injection into 8-week-old male mice as described[41]. Thereafter, kidney samples were harvested 1, 2, and 4 h after NMN injection, and tissues were examined by confocal microscopy using an LSM 510 Zeiss microscope. Fluorescence was detected at 430–480 nm with excitation at 364 nm to detect the signal of Mant. To confirm whether positive signals of Mant-NMN conformed with PTs or podocytes, sequential sections were used for immunofluorescence staining of kidney sections. The primary antibodies used for immunofluorescence studies were anti-AQP1 (a PT marker) (Santa Cruz Biotechnology) and anti-podocin (a podocyte marker) (Sigma-Aldrich).

Human renal specimens from needle biopsy—Needle renal biopsy specimens were obtained from 11 subjects with diabetic nephropathy. No subjects received steroids or immunosuppressive drugs before renal biopsy. As controls, pre-transplant biopsies from five living donors were obtained. Clinical data from the subjects were documented at the time of renal biopsy and are summarized in Supplementary Table 3. The value of eGFR was calculated with a revised MDRD equation for the Japanese population: eGFR (ml min^{-1} 1.73 m^{-2}). Human kidney samples were collected from renal biopsies at Japanese Red Cross Shizuoka Hospital. Written informed consent was obtained from all participants. The study was performed in accordance with the declaration of Helsinki, and the study protocol was approved by the Human Ethics Review Committee of Japanese Red Cross Shizuoka Hospital. Immunohistochemistry for Sirt1 or Claudin-1 was performed on each human sample essentially as described previously. Results are reported as the labeling index, which represents the percentage of total glomerular tuft area that was stained.

Statistical analysis—Data are expressed as means ± s.e.m. Data were analyzed using one- or two-way analysis of variance, as appropriate, followed by Bonferroni's multiple comparison post hoc test. P values < 0.05 were considered statistically significant.

Supplementary Material

Refer to Web version on PubMed Central for supplementary material.

Acknowledgments

REFERENCES

1. Roxburgh SA, et al. Allelic depletion of grem1 attenuates diabetic kidney disease. Diabetes. 2009; 58:1641–1650. [PubMed: 19401426]

2. Rodgers JT, et al. Nutrient control of glucose homeostasis through a complex of PGC-1alpha and SIRT1. Nature. 2005; 434:113–118. [PubMed: 15744310]

3. Bordone L, Guarente L. Calorie restriction, SIRT1 and metabolism: understanding longevity. Nature Rev. Mol. Cell Bio. 2005; 6:298–305. [PubMed: 15768047]

4. Purushotham A, et al. Hepatocyte-specific deletion of SIRT1 alters fatty acid metabolism and results in hepatic steatosis and inflammation. Cell Metab. 2009; 9:327–338. [PubMed: 19356714]

5. Wang RH, et al. Hepatic Sirt1 deficiency in mice impairs mTorc2/Akt signaling and results in hyperglycemia, oxidative damage, and insulin resistance. J. Clin. Invest. 2011; 121:4477–4490. [PubMed: 21965330]

6. Moynihan KA, et al. Increased dosage of mammalian Sir2 in pancreatic beta cells enhances glucose-stimulated insulin secretion in mice. Cell Metab. 2005; 2:105–117. [PubMed: 16098828]

7. Kume S, et al. Calorie restriction enhances cell adaptation to hypoxia through Sirt1-dependent mitochondrial autophagy in mouse aged kidney. J. Clin. Invest. 2010; 120:1043–1055. [PubMed: 20335657]

8. He W, et al. Sirt1 activation protects the mouse renal medulla from oxidative injury. J. Clin. Invest. 2010; 120:1056–1068. [PubMed: 20335659]

9. Kitada M, Kume S, Imaizumi N, Koya D. Resveratrol improves oxidative stress and protects against diabetic nephropathy through normalization of Mn-SOD dysfunction in AMPK/SIRT1-independent pathway. Diabetes. 2011; 60:634–643. [PubMed: 21270273]

10. Tikoo K, Singh K, Kabra D, Sharma V, Gaikwad A. Change in histone H3 phosphorylation, MAP kinase p38, SIR 2 and p53 expression by resveratrol in preventing streptozotocin induced type I diabetic nephropathy. Free Radic. Res. 2008; 42:397–404. [PubMed: 18404539]

11. Kitada M, et al. Dietary restriction ameliorates diabetic nephropathy through anti-inflammatory effects and regulation of the autophagy via restoration of Sirt1 in diabetic Wistar fatty (fa/fa) rats: a model of type 2 diabetes. Exp Diabetes Res. 2011; 2011:908185. [PubMed: 21949662]

12. Xu Y, et al. Resveratrol protects against hyperglycemia-induced oxidative damage to mitochondria by activating SIRT1 in rat mesangial cells. Toxicol. Appl. Pharmacol. 2012; 259:395–401. [PubMed: 22015446]

13. Hasegawa K, et al. Sirt1 protects against oxidative stress-induced renal tubular cell apoptosis by the bidirectional regulation of catalase expression. Biochem. Biophys. Res. Commun. 2008; 372:51–56. [PubMed: 18485895]

14. Hasegawa K, et al. Kidney-specific overexpression of Sirt1 protects against acute kidney injury by retaining peroxisome function. J. Biol. Chem. 2008; 285:13045–13056. [PubMed: 20139070]

15. Gilbert RE, Cooper ME. The tubulointerstitium in progressive diabetic kidney disease: more than an aftermath of glomerular injury? Kidney Int. 1999; 56:1627–1637. [PubMed: 10571771]

16. Nedachi T, Kadotani A, Ariga M, Katagiri H, Kanzaki M. Ambient glucose levels qualify the potency of insulin myogenic actions by regulating SIRT1 and FoxO3a in C2C12 myocytes. Am. J. Physiol. Endocrinol. Metab. 2008; 294:E668–E678. [PubMed: 18230695]

17. Orimo M, et al. Protective role of SIRT1 in diabetic vascular dysfunction. Arterioscler. Thromb. Vasc. Biol. 2009; 29:889–894. [PubMed: 19286634]

18. Gibb DM, et al. Renal tubular proteinuria and microalbuminuria in diabetic patients. Arch Dis Child. 1989; 64:129–134. [PubMed: 2923463]

19. Vaidya VS, et al. Regression of microalbuminuria in type 1 diabetes is associated with lower levels of urinary tubular injury biomarkers, kidney injury molecule-1, and N-acetyl-β-D-glucosaminidase. Kidney Int. 2011; 79:464–470. [PubMed: 20980978]

20. Bonventre JV. Can we target tubular damage to prevent renal function decline in diabetes? Semin Nephrol. 2012; 32:452–462. [PubMed: 23062986]

21. Ohse T, et al. De novo expression of podocyte proteins in parietal epithelial cells during experimental glomerular disease. Am J Physiol Renal Physiol. 2010; 298:F702–F711. [PubMed: 20007346]

22. Zhang J, et al. De novo expression of podocyte proteins in parietal epithelial cells in experimental aging nephropathy. Am J Physiol Renal Physiol. 2012; 302:F571–F580. [PubMed: 22129965]

23. Huby AC, et al. Restoration of podocyte structure and improvement of chronic renal disease in transgenic mice overexpressing renin. PLoS. One. 2009; 4:e6721. [PubMed: 19696925]

24. Ohse T, et al. A new function for parietal epithelial cells: a second glomerular barrier. Am. J. Physiol. Renal. Physio. 2009; 297:F1566–F1574.

25. Rincon-Choles H, et al. ZO-1 expression and phosphorylation in diabetic nephropathy. Diabete. 2006; 55:894–900.

26. Zhang Y, et al. Therapeutic approach for diabetic nephropathy using gene delivery of translocase of inner mitochondrial membrane 44 by reducing mitochondrial superoxide production. J. Am. Soc. Nephrol. 2006; 17:1090–1101. [PubMed: 16510762]

27. Dai C, Stolz DB, Kiss LP, Monga SP, Holzman LB, Liu Y. Wnt/beta-catenin signaling promotes podocyte dysfunction and albuminuria. J Am Soc Nephrol. 2009; 20:1997–2008. [PubMed: 19628668]

28. Punita, Dhawan, et al. Claudin-1 regulates cellular transformation and metastatic behavior in colon cancer. J Clin Invest. 2005; 115:1765–1776. [PubMed: 15965503]

29. Leelahavanichkul A, et al. Angiotensin II overcomes strain-dependent resistance of rapid CKD progression in a new remnant kidney mouse model. Kidney Int. 2010; 78:1136–1153. [PubMed: 20736988]

30. Boireau S, et al. DNA-methylation-dependent alterations of Claudin-4 expression in human bladder carcinoma. Carcinogenesis. 2007; 28:246–258. [PubMed: 16829686]

31. Turek-Plewa J, Jagodzi ski PP. The role of mammalian DNA methyltransferases in the regulation of gene expression. Cell. Mol. Biol. Lett. 2005; 10:631–647. [PubMed: 16341272]

32. Fuks F. DNA methylation and histone modifications: teaming up to silence genes. Curr. Opin. Genet. Dev. 2005; 15:490–495. [PubMed: 16098738]

33. Peng L, et al. SIRT1 deacetylates the DNA methyltransferase 1 (DNMT1) protein and alters its activities. Mol. Cell. Biol. 2011; 31:4720–4734. [PubMed: 21947282]

34. O'Hagan HM, Mohammad HP, Baylin SB. Double strand breaks can initiate gene silencing and SIRT1-dependent onset of DNA methylation in an exogenous promoter CpG island. PLoS. Genet. 2008; 4:e1000155. [PubMed: 18704159]

35. Zhang Q, et al. Metabolic regulation of SIRT1 transcription via a HIC1:CtBP corepressor complex. Proc. Natl. Acad. Sci. U. S. A. 2007; 104:829–833. [PubMed: 17213307]

36. Wang P, et al. Nicotinamide phosphoribosyltransferase protects against ischemic stroke through SIRT1-dependent adenosine monophosphate-activated kinase pathway. Ann. Neurol. 2011; 69:360–374. [PubMed: 21246601]

37. Ramsey KM, et al. Age-associated loss of Sirt1-mediated enhancement of glucose-stimulated insulin secretion in beta cell-specific Sirt1-overexpressing (BESTO) mice. Aging Cell. 2008; 7:78–88. [PubMed: 18005249]

38. Wang P, et al. Perivascular adipose tissue-derived visfatin is a vascular smooth muscle cell growth factor: role of nicotinamide mononucleotide. Cardiovasc. Res. 2009; 81:370–380. [PubMed: 18952695]

39. Formentini L, Moroni F, Chiarugi A. Detection and pharmacological modulation of nicotinamide mononucleotide (NMN) in vitro and in vivo. Biochem. Pharmacol. 2009; 77:1612–1620. [PubMed: 19426698]

40. Taha HM, et al. Molecular analysis of the interaction of anthrax adenylyl cyclase toxin, edema factor, with 2′(3′)-O-(N-(methyl)anthraniloyl)-substituted purine and pyrimidine nucleotides. Mol. Pharmacol. 2009; 75:693–703. [PubMed: 19056899]

41. Lai LW, Moeckel GW, Lien YH. Kidney-targeted liposome-mediated gene transfer in mice. Gene Ther. 1997; 4:426–431. [PubMed: 9274719]

42. Zhang Z, et al. Regulated ATP release from astrocytes through lysosome exocytosis. Nat. Cell Biol. 2007; 9:945–953. [PubMed: 17618272]

43. Peng L, Yuan Z, Ling H, Fukasawa K, Robertson K, Olashaw N, Koomen J, Chen J, Lane WS, Seto E. Sirt1 deacetylates the DNA methyltransferase 1 (Dnmt1) protein and alters its activities. Mol Cell Biol. 2011; 31:4720–4734. [PubMed: 21947282]

44. Zorzano A, Zorzano A, Hernández-Alvarez MI, Palacín M, Mingrone G. Alterations in the mitochondrial regulatory pathways constituted by the nuclear co-factors PGC-1alpha or PGC-1beta and mitofusin 2 in skeletal muscle in type 2 diabetes. Biochim. Biophys. Acta. 2010; 1797:1028–1033. [PubMed: 20175989]

45. Clodfelder-Miller B, Sarno PD, Zmijewska AA, Song L, Jope RS. Physiological and pathological changes in glucose regulate brain Akt and glycogen synthase kinase-3. J. Biol. Chem. 2005; 280:39723–39731. [PubMed: 16179343]

46. Leotlela PD, et al. Claudin-1 overexpression in melanoma is regulated by PKC and contributes to melanoma cell motility. Oncogene. 2007; 26:3846–3856. [PubMed: 17160014]

47. Moeller MJ, Sanden SK, Soofi A, Wiggins RC, Holzman LB. Podocyte-specific expression of cre recombinase in transgenic mice. Genesis. 2003; 35:39–42. [PubMed: 12481297]

48. Sung SH, et al. Blockade of vascular endothelial growth factor signaling ameliorates diabetic albuminuria in mice. J. Am. Soc. Nephrol. 2006; 17:3093–3104. [PubMed: 16988063]

49. Cohen CD, et al. Laser microdissection and gene expression analysis on formaldehyde-fixed archival tissue. Kidney Int. 2002; 61:125–132. [PubMed: 11786092]

50. Kohda Y, et al. Analysis of segmental renal gene expression by laser capture microdissection. Kidney Int. 2000; 57:321–331. [PubMed: 10620215]

51. Asanuma K, Campbell KN, Kim K, Faul C, Mundel P. Nuclear relocation of the nephrin and CD2AP-binding protein dendrin promotes apoptosis of podocytes. Pro. Natl. Acad. Sci. U.S.A. 2007; 104:10134–10139.

52. Terasawa K, et al. Epigenetic inactivation of TMS1/ASC in ovarian cancer. Clin. Cancer. Res. 2004; 10:2000–2006. [PubMed: 15041718]
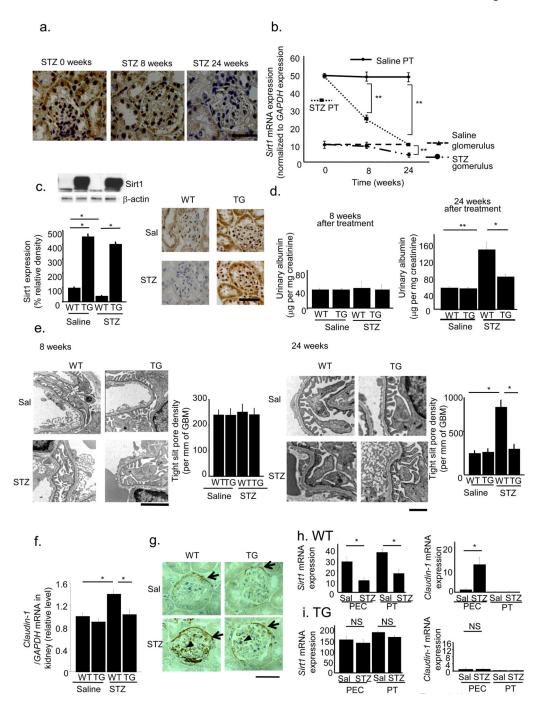
Figure 1.
Alleviation of albuminuria in diabetes-induced albuminuria in transgenic (TG) mice with proximal tubule (PT)-specific Sirt1 overexpression. **(a,b)** Temporal changes in *Sirt1* expression 0, 8, and 24 weeks after streptozotocin (STZ) treatment in wild-type (WT) mice. **(a)** Immunostaining for Sirt1 in the kidney. The scale bar represents 50 μm. **(b)** *Sirt1* mRNA expression levels normalized to that of *GAPDH* in PT and glomeruli of saline- or STZ-treated mice. **(c)** Immunoblotting (left) and immunostaining (right) for Sirt1 expression in the kidneys of TG and WT mice treated with saline (Sal) or STZ at 24 weeks after STZ

treatment. Sirt1 band in TG mice consisted of a band for endogenous mouse Sirt1 (100 kDa) and one for FLAG-tagged overexpressed human Sirt1 (101 kDa). Band intensity was normalized to that for β-actin. Scale bar, 50 μm. (**d**) Urinary albumin excretions at 8 weeks (left) and 24 weeks (right) after STZ treatment. (**e**) Representative electron photomicrographs 8 weeks (left) and 24 weeks (right) after STZ treatment. Bar graphs represent the tight slit pore densities. Scale bar, 500 nm. (**f**) The mRNA levels for *Claudin-1*. (**g**) Immunostaining for Claudin-1. Arrows indicate stained PECs. Triangles indicate stained cells in the glomeruli. Bars, 50 μm. (**h,i**) The expression of *Sirt1* (left) and *Claudin-1* (right) mRNA in micro-dissected parietal epithelial cells (PECs) and proximal tubules (PT) of WT mice (**h**) and TG mice (**i**) treated with saline or STZ. $**P < 0.01$, $*P < 0.05$, $n = 8$.
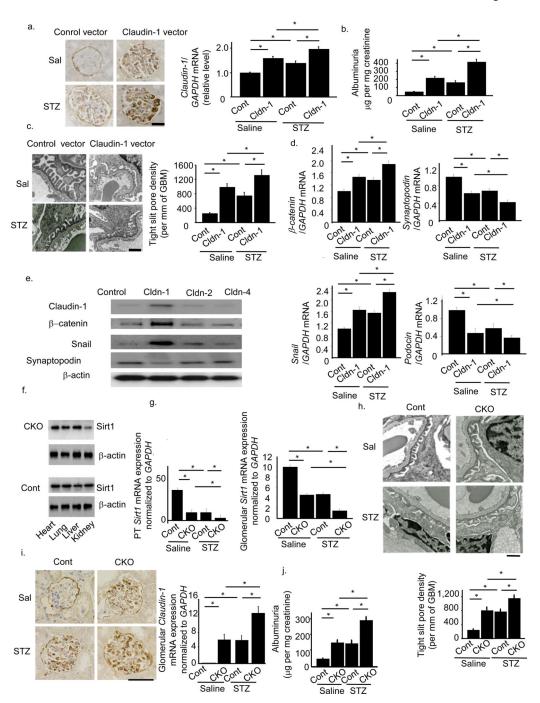
Figure 2.
Direct effects of Claudin-1 on podocytes, mice with streptozotocin-induced diabetes, and the phenotypes of proximal tubule (PT)-specific Sirt1 knockout mice. (**a**) Claudin-1 staining after intravenous injection of *NPHS2-Claudin-1* (Cldn-1) or control vector (Cont) into saline (Sal)-treated or streptozotocin (STZ)-treated mice. The right panel shows mRNA expression for *Claudin-1*. Scale bar, 50 μm. (**b**) Albuminuria in Cont+Sal, Cldn-1+Sal, Cont+STZ and Cldn-1+STZ mice. (**c**) Electron photomicrographs of kidneys from mice in each experimental group. The bar graph shows tight slit pore densities. Scale bar, 500 nm. (**d**)

Expression levels for *Claudin-1*, β-*catenin, Snail, Synaptopodin*, and *Podocin* mRNAs in micro-dissected glomeruli in all four groups of mice. (**e**) Immunoblotting analysis for the expression of Claudin-1, β–catenin, Snail, and Synaptopodin in cultured podocytes transfected with expression vectors for Claudin-1, Claudin-2, Claudin-4 or empty vector pcDNA3. (**f**) Production of PT-specific *Sirt1$^{-/-}$* (conditional knockout, CKO) mice. Immunoblotting analysis for Sirt1 expression in the heart, lung, liver, and kidney of CKO and control (Cont) mice. (**g**) Expression of *Sirt1* in PTs (left) and glomeruli (right) of CKO and Cont mice (**h**) Electron photomicrographs of a kidney in STZ-treated CKO and control mice. The bar graph shows quantification of tight slit pore densities. Scale bar, 500 nm. (**i**) Immunostaining for Claudin-1 in kidneys (left) and mRNA expression for *Claudin-1* in micro-dissected glomeruli (right) from Cont+Sal, Cont+STZ, CKO+Sal and CKO+Sal mice. Scale bar, 50 μm. (**j**) Albuminuria in each experimental group. *$P < 0.05$, $n = 8$.
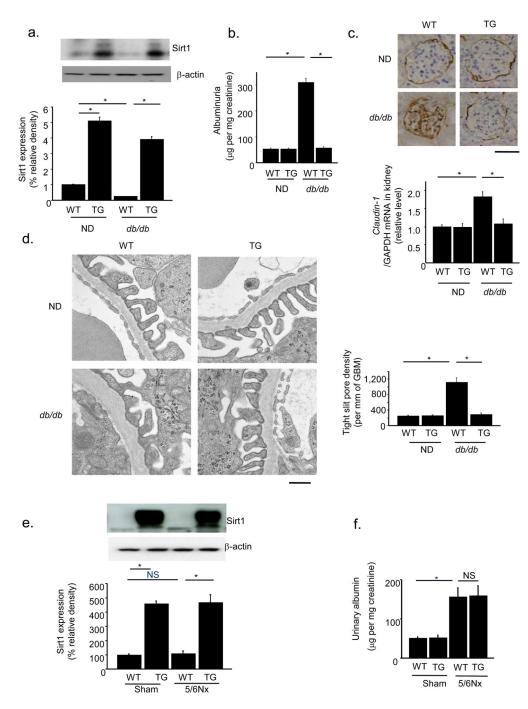
Figure 3.
Proximal tubule-specific Sirt1 overexpression alleviates diabetic albuminuria in *db/db* mice
but not in 5/6th nephrectomized (5/6Nx) mice. (**a**) Immunoblotting for Sirt1 in the kidneys
of TG mice and wild-type littermates (WT) crossed with *db/db* or non-diabetic mice (ND).
The lower panel shows the results of densitometry analysis of band intensity. (**b**)
Albuminuria in WT-ND, TG-ND, WT-*db/db* and TG-*db/db* mice. (**c**) Immunostaining for
Claudin-1 in kidneys from each experimental group. The lower panel shows mRNA
expression for *Claudin-1*. Scale bar, 50 μm. (**d**) Electron photomicrographs of a kidney from

each mice group (left). The bar graph (right) shows the tight slit pore densities. Scale bar, 500 nm. (**e**) Immunoblotting for Sirt1 in the kidneys of TG and WT mice after 5/6Nx or sham operation. The lower panel shows densitometry analysis of band intensity. (**f**) Albuminuria in TG and WT mice after 5/6Nx or sham operation. *$P < 0.05$, $n = 8$.
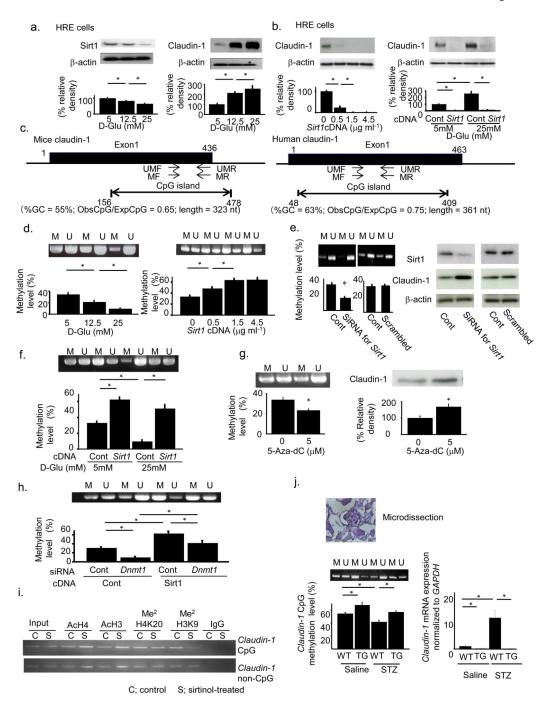
Figure 4.

Epigenetic regulation of *Claudin-1* gene expression by Sirt1. (**a**) Effects of glucose concentration on the expression of Sirt1 (left) and Claudin-1 (right). (**b**) Effects of Sirt1 overexpression (left) and combined effects of glucose and Sirt1 (right) on Claudin-1 expression. (**c**) CpG islands and positions of primers for methylated (MF and MR) and unmethylated (UMF and UMR) genes on the *Claudin-1* gene of mice (left) and human (right). (**d**) Effects of glucose concentration (left) and Sirt1 overexpression (right) on *Claudin-1* gene methylation. (**e**) Effects of transfection with siRNA for *Sirt1* on *Claudin-1*

gene methylation (left) and Claudin-1 protein expression (right). (**f**) Combined effects of glucose and Sirt1 on *Claudin-1* gene methylation. (**g**) Methylation of *Claudin-1* gene (left) and the level of Claudin-1 protein (right) after treatment with the DNA methyltransferase (Dnmt) inhibitor 5-aza-dC. (**h**) Methylation of the *Claudin-1* gene with or without transfection with Sirt1 expression vectors or *Dnmt1* siRNA. (**i**) ChIP assays using HRE cells cultured with sirtinol (S, 20 mM) or vehicle (C). Antibodies against acetylated histone 4 (AcH4), acetylated histone 3 (AcH3), dimethylated H4K20 (Me^2H4K20), and dimethylated H3K9 (Me^2H3K9) were used. (**j**) *Claudin-1* CpG methylation in the kidneys of TG mice treated with or without streptozotocin (STZ). Left; Methylation-specific PCR and real-time methylation-specific PCR using micro-dissected PECs. Right; *Claudin-1* mRNA expression in PECs. (**d,e,f,g,h,j**) M indicates methylated DNA and U unmethylated DNA. *$P < 0.05$, $n = 5$.
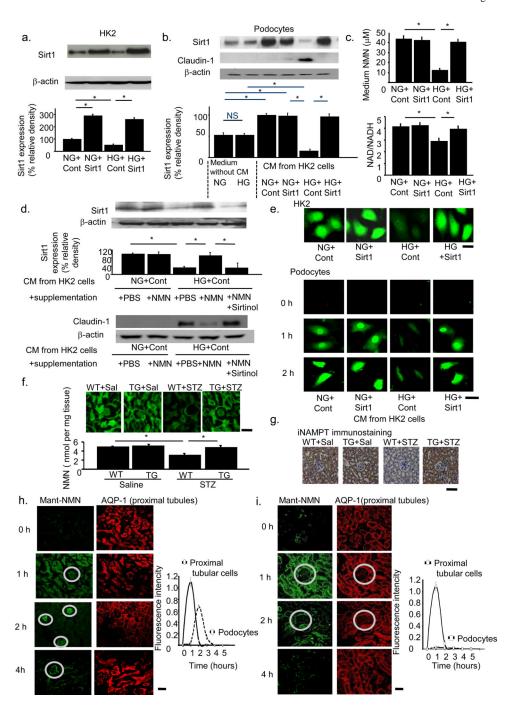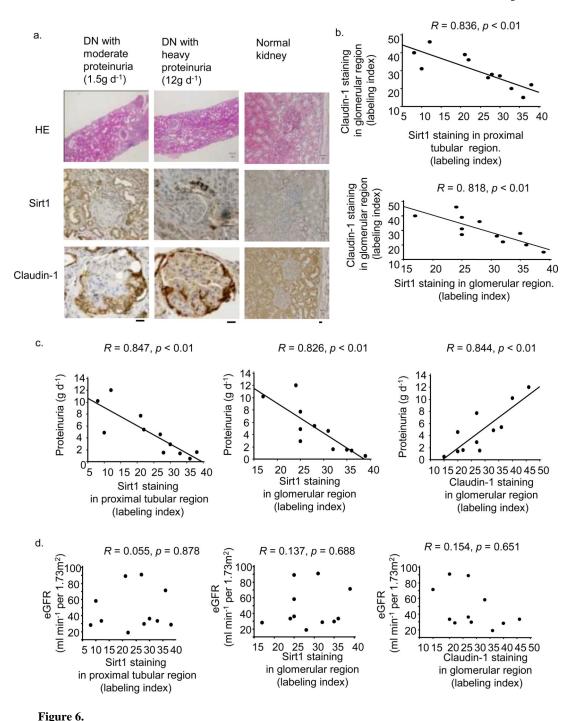
Figure 5.
Evidence for the retrograde interplay from tubular cells to podocytes. (**a**) HK-2 cells were cultured under the four conditions of NG (normal glucose)+Cont (control vector), NG+Sirt1 (*Sirt1* expression vector), HG (high glucose)+Cont and HG+Sirt1. Immunoblotting for Sirt1 (upper) and densitometry analysis (lower). (**b**) Sirt1 (upper) and Claudin-1 (lower) expression in podocytes cultured in conditioned medium (CM) from each of the above four experimental conditions or in NG or HG conditions without CM. (**c**) NMN concentrations (upper) and NAD/NADH ratio (lower) of each CM. (**d**) Sirt1 (upper) and Claudin-1 (lower)

expression in podocytes cultured in each CM supplemented with NMN, phosphate-buffered saline (PBS), or sirtinol. (**e**) Intracellular autofluorescence of NMN in HK-2 cells (upper) and podocytes (lower) at 0, 1, and 2 h after CM transfer. CM were from the four conditions of HK-2 cell culture media. Scale bar, 20 μm. (**f,g**) Tissue NMN concentrations (**f**) and iNAMPT immunostaining (**g**) of kidneys from proximal tubule-specific *Sirt1* transgenic (TG) mice and wild-type littermates (WT) mice 24 weeks after treatment with saline (Sal) or streptozotocin (STZ). Scale bar, 50 μm. (**h,i**) Representative confocal images for Mant fluorescence in normal (**h**) and PT-specific *Sirt1*-deficient mice (**i**). Mant-NMN (green, left) was detected at 0, 1, 2, 4 h after injection. Sequential sections were stained with anti-AQP-1 antibody (**h,i**; right). Glomeruli are indicated in circles. Temporal profiles of the mean Mant-NMN intensity in tubular and podocyte regions are shown in the graph, $n = 5$. *$P < 0.05$, $n = 5$. Scale bar, 50 μm.

Figure 6.
Glomerular Sirt1 or Claudin-1 immunostaining in human renal biopsy specimens. (**a**) Representative photomicrograph of HE staining or immunostaining for Sirt1 and Claudin-1 in needle renal biopsy specimens of subjects with diabetic nephropathy (DN) (sample names: DN-3 and 6, Supplementary Table 3) and a control (sample name: CO-1). Bars; 50 nm. (**b**) The relationship between immunostaining for Claudin-1 and that for Sirt1 in the proximal tubular region (upper) and glomerular region (lower) in renal biopsy specimens from subjects with DN, $n = 11$. (**c**) The relationships between proteinuria and

immunostaining for proximal tubular Sirt1 (left), glomerular Sirt1 (middle), and Claudin-1 (right), $n = 11$. (**d**) The relationships between eGFR and immunostaining for proximal tubular Sirt1 (left), glomerular Sirt1 (middle) and Claudin-1 (right), $n = 11$.